3
Computational Industrial Mechanics Programmes (CIMP)

Highlights

Finite element simulations and the some of the basic isseus in their application and validation constitute one primary focus of CIMP. The other major area of activity is modelling and simulation of the complex industrial flows. A number os important results have emerged in 2006-07.

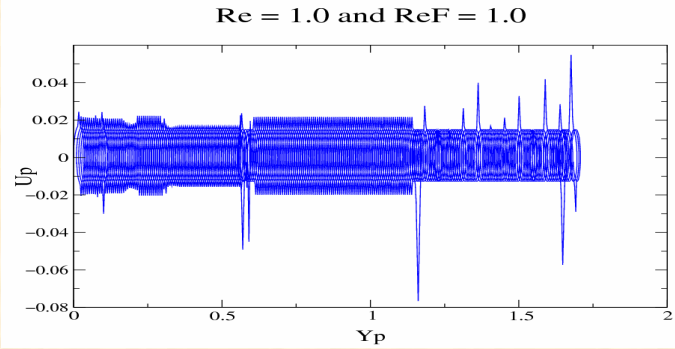

Inside

3.1 Field-consistency aspects of locking in a geometrically non-linear beam formulation

Discretisation errors that appear uniquely in a non-linear beam formulation due to the presence of non-linear derivative terms in the membrane strain term in the form of degraded performance (locking) and spurious stress oscillations can be interpreted using the field-consistency paradigm. The errors are seen to separate out into the usual discretisation errors and that of a field-inconsistency origin. Numerical experiments with a simple beam element show that reduced integration can be used to remove the field-inconsistency errors. Also, it is seen that the locking errors contribute to both local and global (pollution) error. An optimal stress recovery strategy where spurious stress due to field-inconsistency is present is also recommended.

The phenomenon of locking (in the form of delayed convergence and spurious stress oscillations) is quite well known for linear formulations. However, there are very few studies on locking type behaviour in non-linear problems.

The bending of beams with moderately large rotations (von Karman theory) can be described within the context of the classical Euler-Bernoulli (EB) theory by writing the strains ε (extensional or membrane) strain and κ (curvature) in terms of u and w which are the in-plane (axial) and transverse displacements. The non-linear stiffness matrices can then be set up quite easily following standard procedures and a direct iteration or Newton-Raphson method can be used to obtain solutions to the non-linear problem.

It is well known that the simplest 2-node linear EB element based on linear functions for u and cubic functions for w is free of locking and produces excellent displacements and stress predictions. However, both Kikuchi and Aizawa, and Reddy have reported that if the non-linear formulation uses the conventional 2 pt. Gaussian integration rule to compute all stiffness matrices (i.e. linear and non-linear), the convergence is noticeably poor. This was attributed to membrane locking and it was shown that by using a 2 pt. rule for the bending energy and a reduced 1 pt. rule for the membrane energy, excellent results were obtained. We can re-interpret this from the field-consistency angle to show that only the constant term is consistently constituted to model inextensional bending. Thus, only a 1 pt. integration of the extensional strain will preserve this consistency. A higher order rule, say the 2 pt. rule which is conventionally used for the formulation, will retain the higher order terms, thus leading to poor convergence, and higher order stress oscillations. Our numerical examples below highlight these points very clearly.

Consider a uniform beam of length L = 100, cross section dimensions of 1 x 1, made of a material with $E = 30 \times 10^6$ that is simply supported at both ends subjected to a uniformly distributed load of intensity q per unit length. The units are consistently chosen, so that the exact deflection at the middle of the beam in linear bending theory is 0.5208, when $q = 1$. In linear bending theory, where the beam is assumed to undergo pure bending (i.e. there is no axial deformation), it is immaterial to consider whether the beam is allowed free movement in the axial direction (i.e. u) at the supported ends. However, in non-linear bending, this is a crucial distinction. We shall therefore designate by the hinged-hinged (HH) condition, the case where there is no axial restraint at both ends, Here, we have inextensional bending, which is largely of a linear nature.

The HH case is ideal to test the consistency aspect of the problem. As a non-linear beam element formulation is being used, a correct model should be able to recover the purely linear bending response under increasing load. This is possible only if the element can ensure that the inextensional axial condition (i.e. as there is no axial restraint at both

ends, no axial force should develop) is consistently recovered throughout. We shall use two versions of the EB element. The EB2x2 element which will have locking uses 2 pt. integration for bending energy and extensional energy while the EB2x1 element which will be lock free according to our foregoing analysis will use 2 pt. integration for bending energy but only 1 pt. integration for the extensional energy. Using symmetry, half of the beam is modeled with equal length elements.

Table 3.1. Central deflections for a Hinged-Hinged Beam under uniformly distributed load where half the beam is modeled with four equal length EB beam elements.

q	Present		Reddy [9]	
	2x2	2x1	2x2	2x1
1	0.5108	0.5208	0.5108	0.5208
2	0.9738	1.0417	0.9739	1.0417
3	1.3764	1.5625	1.3764	1.5625
4	1.7265	2.0833	1.7265	2.0833
5	2.0351	2.6042	2.0351	2.6042
6	2.3115	3.1250	2.3116	3.1250
7	2.5624	3.6458	2.5630	3.6458
8	2.7926	4.1667	2.7930	4.1667
9	3.0060	4.6875	3.0060	4.6875
10	3.2051	5.2083	3.2051	5.2083

Table 3.1 shows the deflection under the load as q increases from 1 to 10, when half of the beam is modeled with four equal length elements. Results from Reddy are also shown. It is clear that the EB2x1 model is able to capture the linear behaviour exactly but the EB2x2 model shows an additional stiffening due to the inability of the model to capture the zero axial force consistently due to the presence of the inconsistent terms. Figure 3.1 shows the variation of axial force for $q = 1$ when half of the HH beam is modeled with 2 EB2x1 elements. It is seen that when the axial force is sampled at the Gauss point, it predicts the exact zero value expected accurately. Also shown for effect is the

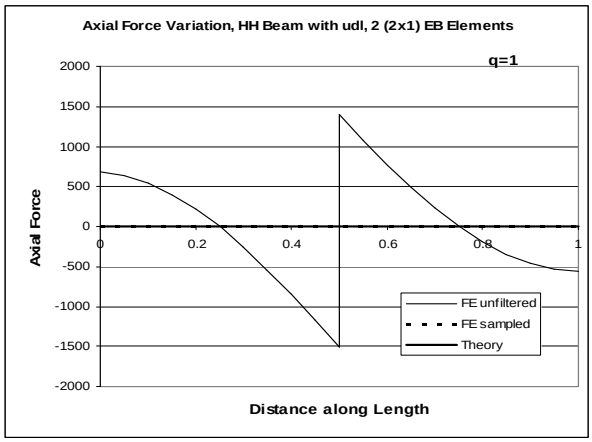

Figure 3.1. The variation of axial force for $q = 1$ when half of the HH beam is modeled with 2 EB2x1 elements

complex quartic variation in N which accounts for the additional stiffening effect seen if a 2x2 integration strategy is used.

R Murali and G Prathap

3.2 Mesh distortion, locking and the use of metric trial functions for displacement type finite elements

The use of metric trial functions to represent the real stress field in what is called the unsymmetric finite element formulation is an effective way to improve predictions from distorted finite elements. This approach works surprisingly well because the use of parametric functions for the test functions satisfies the continuity conditions while the use of metric (Cartesian) shape functions for the trial functions ensures that the stress representation during finite element computation can retrieve in a best-fit manner, the actual variation of stress in the metric space. However, the issue of how to handle situations where there is locking along with mesh distortion has never been addressed. We have shown that the use of a consistent definition of the constrained strain field along with the unsymmetric approach can ensure a lock-free solution even when

there is mesh distortion. The three-noded Timoshenko beam element is used to illustrate the principles. Some significant conclusions are drawn regarding the optimal strategy for finite element modelling where distortion effects and field-consistency requirements have to be reconciled simultaneously.

Surendra Kumar and Gangan Prathap

3.3 Impact response and damage in curved composite laminates

The impact response and the impact-induced damage in curved composite laminate subjected to transverse impact by a metallic impactor are studied using three-dimensional finite element method. Several example problems of graphite/epoxy cylindrical shell are considered and effects of impactor parameter (impactor velocity and impactor mass) and laminate characteristics (shell curvature and fibre orientation of plies) are established. Impact- induced damages (matrix cracking and delamination) are predicted using appropriate three-dimensional stress-based failure criteria. In order to take account of degradation of material due to damage during the impact, the stiffness matrix of the failed region of the laminate is reduced as the solution progresses.

Surendra Kumar, B N Rao and B Pradhan

3.4 Making sense of the Quadrilateral Area Coordinate membrane elements

For a half-century, one of the demanding challenges in finite element research has been the search for robust quadrilateral membrane elements which can pass the patch test, remove parasitic shear and Poisson's ratio stiffening, and are insensitive to mesh distortion. This requires the delicate balancing of continuity requirements and completeness requirements. The isoparametric quadrilateral membrane elements satisfy the continuity requirements always. In rectangular form, they perform extremely well, except in cases where parasitic shear is involved. So their poor performance when the elements are used in general (i.e. distorted) quadrilateral form is now attributed to the failure to accommodate the completeness requirements.

The Quadrilateral Area Coordinates (QAC) approach is a compromise that tries to use shape functions which are in physical space, but as these cannot ensure exact continuity, require a relaxed generalized continuity to be be imposed. AGQ6-I and AGQ6-II are the two versions of the 4-node membrane elements combine the area coordinate approach with generalized conforming conditions. The constant stress strong patch test, the linear stress bending strong patch test and the bilinear stress bending strong

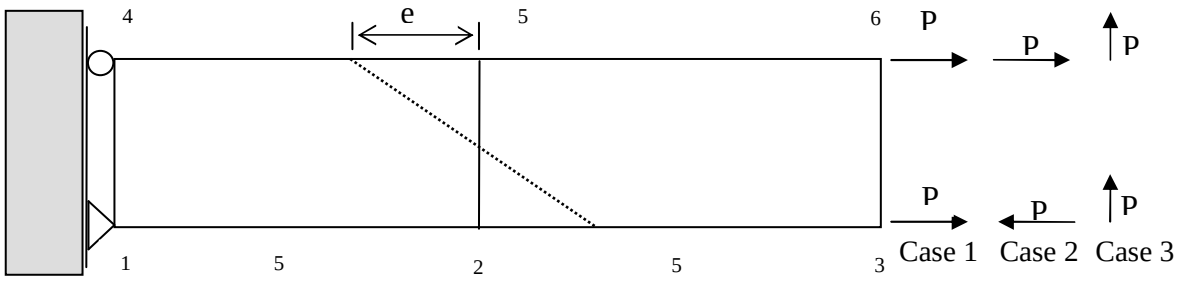

Figure 3.2. Two element patch test for cantilever beam with distortion parameter – various load cases

patch test have been considered to assess the QAC elements performance, corresponding to the three load cases shown in Figure 3.2.

The simplest patch for a plane stress problem requires two 4-node quadrilateral membrane elements. The distortion parameter e can be used to move from a rectangular division to a highly distorted mesh division. The beam has dimensions 10 x 2 x 1 and the force at the free end is applied at nodes 3 and 6 equally as P = 0.5. Let the material properties be E = 75 and ν = 0.25.

Table 3.2 Normalized deflections (u for axial force and v for end moment case) at nodes 3 and 6 for cantilever beam

e	u for axial force (case 1)		v for end moment (case 2)	
	AGQ6-I	AGQ6-II	AGQ6-I	AGQ6-II
0	1.000	1.000	1.0000	1.0000
1	1.000	1.054	1.0000	1.0000
2	1.000	1.225	1.0000	1.0000
3	1.000	1.544	1.0000	1.0000
4	1.000	2.084	1.0000	1.0000

From Table 3.2, it is seen that the AGQ6-I element passes the constant stress strong patch test. However, the AGQ6-II element fails to pass this test, errors increasing with distortion and going beyond the exact value. From Table 3.2, for the linear bending strong patch test, the AGQ6-I and AGQ6-II elements are both free of Poisson's ratio stiffening and parasitic shear and pass this test with flying colors if only tip deflections are taken into account. That this is not the case will be seen when we examine the deflections at nodes 2 and 5 in Table 3.3.

We have seen that only AGQ6-II passes this criterion exactly. The results from AGQ6-I are in error and these increase with distortion. We see also that as distortion is introduced, the use of simple reduced integration strategies will not eliminate locking. The AGQ6 elements, have introduced bubble functions effectively involving quadratic terms in x and y and so meet the field-consistency criteria (shear strains are complete to linear terms in x and y without introducing inconsistent terms) and are able to eliminate parasitic shear, even where there is distortion. It is this result (Table 3.2) that raised false hopes that the AGQ6 elements have finally ended a long search for the perfect family of membrane elements. Tables 3.2 and 3.3 warn us that the search is not over; the AGQ6-I element fails one patch test and the AGQ6-II fails the other and the partial successes seen are to be taken as fortuitous.

Table 3.3 Normalized deflections v, at nodes 2 and 5 for cantilever beam subjected to end moment

e	Node 2			Node 5		
	Exact	AGQ6-I	AGQ6-II	Exact	AGQ6-I	AGQ6-II
0	0.2500	0.2500	0.2500	0.2500	0.2500	0.2500
1	0.3600	0.3533	0.3600	0.1600	0.1533	0.1600
2	0.4900	0.4633	0.4900	0.0900	0.0633	0.0900
3	0.6400	0.5800	0.6400	0.0400	-0.0200	0.0400
4	0.8100	0.7033	0.8100	0.0100	-0.0967	0.0100

Table 3.4 Normalized deflections v, at node 3 for cantilever beam subjected to shear force

e	exact	v for shear force (case 3)	
		AGQ6-I	AGQ6-II
0	1.0000	0.9396	0.9396
1	1.0000	0.9545	0.9650
2	1.0000	0.9999	1.0520
3	1.0000	1.0808	1.2370
4	1.0000	1.2105	1.5916

From Table 3.4 we have seen that both versions of the area coordinate generalized conforming elements give higher answers as distortion increases for the bilinear bending strong patch test (Case 3). The use of area coordinates is a proxy for the use of metric functions and so completeness is achieved in physical space and not in natural space. By adding internal functions, completeness to quadratic terms in metric space is provided, but we see that this is not enough. It is known that the strict interpretation of the variational basis for the development of displacement type finite elements leads to a projection theorem and energy-error rules that require variationally correct solutions to have less energy than the exact solution (Tables 3.2, 3.3 and 3.4). Clearly, from this point of view, the area coordinate elements are not governed by the boundedness property. So it has been understood that more needs to be done both in terms of utility and performance and also in terms of understanding the QAC elements.

V Senthilkumar and G Prathap

3.5 Inertial Effects on Forced Particles in Unsteady Flows at Low Reynolds Numbers

The main objectives of the above work are the following:

a) To study the dynamics of periodically forced small particles in a uniform time dependent flow field in the presence of fluid and particle inertia at low Reynolds numbers.

b) To study the rheology of a dilute suspension of a number of such particles at low Reynolds numbers under the action of an external periodic force field.

c) To determine the parametric regions, if any, of such systems where chaos can occur in the dynamics of individual particles and also in the rheological properties of such systems.

The problem was restricted to "The Effect of Inertia on the Dynamics of a Periodically Forced Spherical Particle in a Quiescent Fluid" due to logistic and technical problems during the year 2005-06.

The formalism of Lovalenti and Brady (1993) was used and a formula was obtained for the variation of the velocity and position of the particle moving in a quiescent fluid, along the direction of the external periodic force. Software was developed to study the effect of inertia on the dynamics of a periodically forced spherical particle in a quiescent fluid based on the following formulae:

$$\frac{dY_p}{dt} = \mathrm{U_p}$$

$$\frac{dU_p}{dt} = \frac{1}{\mathrm{Re}^*}\left[\mathrm{Re}_F \sin t - 6\pi U_p + \frac{3}{8}\left(\frac{\mathrm{Re}Sl}{\pi}\right)^{1/2}(J_1 + I_1)\right]$$

Here,

$$\mathrm{Re}^* = \frac{4\pi}{3}\mathrm{Re} + \frac{2\pi}{3}\mathrm{Re}Sl$$

$$\mathrm{Re}_F = \frac{F_0}{\mu a U_c}$$

$$J_1 = 16\pi U_p(t)\left[\frac{1}{\sqrt{t}} - \frac{1}{\sqrt{\varepsilon}}\right]$$

$$I_1 = \int_0^{t-\varepsilon}\left\{\frac{1}{A^2}\left(\frac{\sqrt{\pi}}{2|A|}erf(A) - \exp(-A^2)\right)\right\}\frac{12\pi U_p(s)}{(t-s)^{3/2}}ds$$

$$A = \frac{\mathrm{Re}}{2}\left(\frac{t-s}{\mathrm{Re}\,Sl}\right)^{1/2}\left(\frac{Y_S(t)-Y_S(s)}{t-s}\right)$$

In the current year the software developed for studying the effect of inertia on the dynamics of a periodically forced spherical particle in a quiescent fluid was tested for consistency. There were 3 tests performed.

TEST1: The solution of the problem of a spherical particle of greater density than fluid derived using the assumptions of Reynolds number Re<<1 And Strouhal's number Sl arbitrary is well known from the literature and this solution was reproduced when we assumed that the external force was constant.

TEST2: We assumed that the velocity of the fluid at infinity was a constant ie, $U^{\infty} = U_0$ and we set $Re_F = 0$. Under these assumptions $U_p \rightarrow U_0$ as $t \rightarrow \infty$. This result was obtained from the software.

TEST3: We generated number of outputs using $U_0 = 0$ and $U_0 \neq 0$ and compared the results at $U_0 \rightarrow 0$. We found that the results matched for $U_0 = 0$ and $U_0 \rightarrow 0$.

Thus these tests gave us reasonable confidence in our results.

Various other analyses were performed using the software.

1. The nonlinear term was taken to be zero and in the phase plot between velocity of the particle and position of the particle was obtained to be a limit cycle.

2. The sign of the nonlinear term was changed, which resulted in a change in the direction of the drift velocity.

A large number of solutions were generated for different values of U_0, Re and Re_F. this led to a large number of different patterns of U_p versus Y_p plots which are being analyzed.

Formalism was developed for a non quiescent fluid by considering the velocity of the fluid at infinity as a constant, i.e., $U^{\infty} = U_0$ as:

$$\frac{dY_p}{dt} = \mathrm{U_p}$$

$$\frac{dU_p}{dt} = \frac{1}{\mathrm{Re}^*}\left[\mathrm{Re}_F \sin t - 6\pi(U_p - U_0) + \frac{3}{8}\left(\frac{\mathrm{Re}Sl}{\pi}\right)^{1/2}(J_1 + I_1)\right]$$

Here,

$$J_1 = 16\pi(U_p(t) - U_0)\left[\frac{1}{\sqrt{t}} - \frac{1}{\sqrt{\varepsilon}}\right]$$

$$I_1 = \int_0^{t-\varepsilon}\left\{\frac{1}{A^2}\left(\frac{\sqrt{\pi}}{2|A|}erf(A) - \exp(-A^2)\right)\right\}\frac{12\pi(U_p(s) - U_0)}{(t-s)^{3/2}}ds$$

This has been incorporated in the software and various interesting results and patterns of U_p versus Y_p plots have been obtained.

The important result of this was that the effect of U_0 dominated as the Reynolds number was increased.

Some of the typical patterns of U_p versus Y_p plots are as shown below:

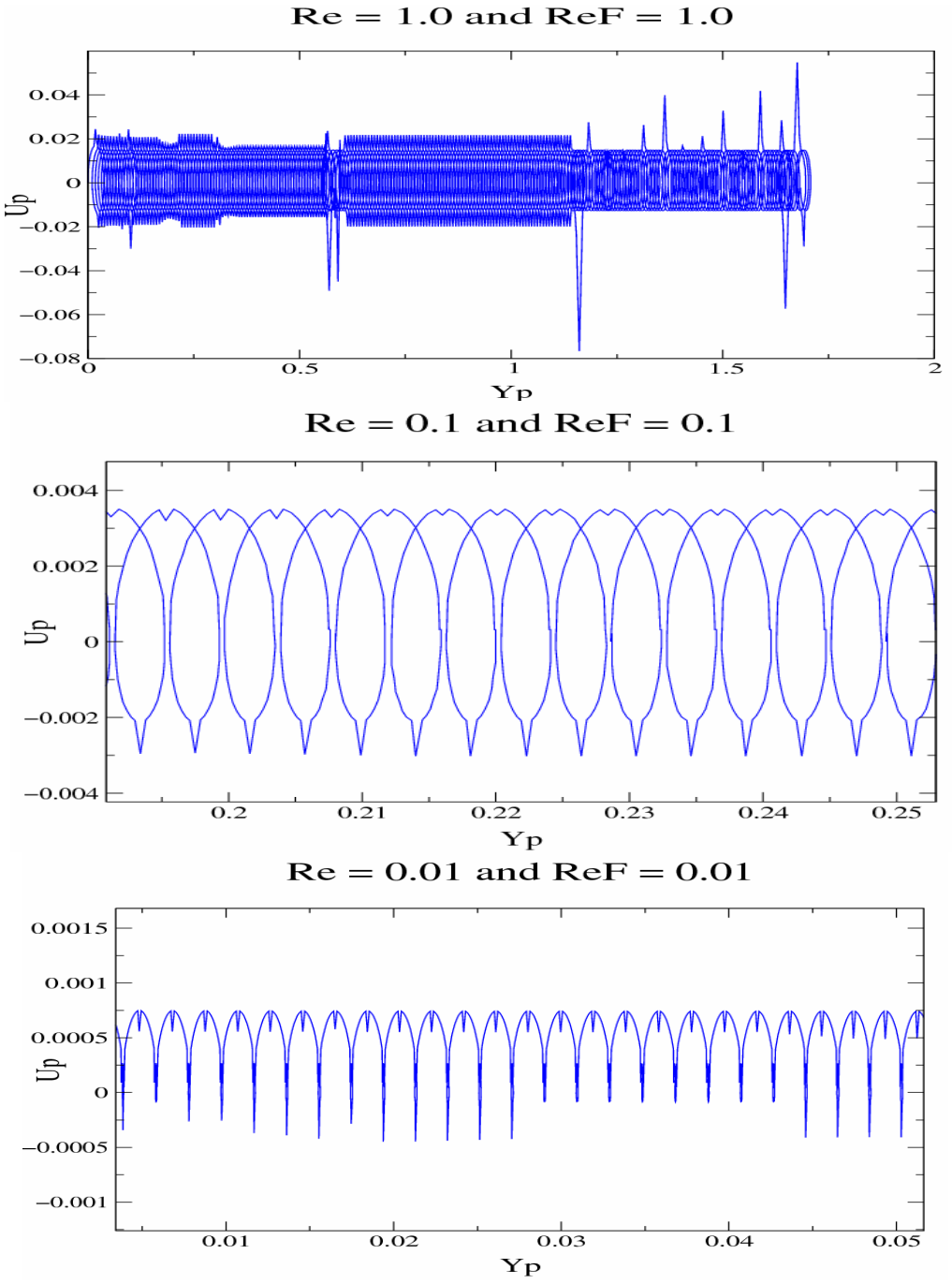

Figue 3.3 Phase plots of U_p for different values of Re and Re_F.